Detailed calibration of the PI-LCX:1300 high performance single photon counting hard x-ray CCD camera*

Wei Hong(洪伟)†, Xian-Lun Wen(温贤伦), Lai Wei(魏来), Bin Zhu(朱斌), Yu-Chi Wu(吴玉迟), Ke-Gong Dong(董克攻), Chun-Ye Jiao(焦春晔), Bo Wu(伍波), Ying-Ling He(何颖玲), Fa-Qiang Zhang(张发强), Wei-Min Zhou(周维民), and Yu-Qiu Gu(谷渝秋)

Science and Technology on Plasma Physics Laboratory, Laser Fusion Research Center, China Academy of Engineering Physics, Mianyang 621900, *China*

(Received 19 October 2016; revised manuscript received 22 November 2016; published online 10 January 2017)

X-ray charge-coupled-device (CCD) camera working in single photon counting mode is a type of x-ray spectrometer with high-sensitivity and superior signal-to-noise performance. In this study, two single photon counting CCD cameras with the same mode (model: PI-LCX: 1300) are calibrated with quasi-monochromatic x-rays from radioactive sources and a conventional x-ray tube. The details of the CCD response to x-rays are analyzed by using a computer program of multi-pixel analyzing and event-distinguishing capability. The detection efficiency, energy resolution, fraction of multi-pixel events each as a function of x-ray energy, and consistence of two CCD cameras are obtained. The calibrated detection efficiency is consistent with the detection efficiency from Monte Carlo calculations with XOP program. When the multi-pixel event analysis is applied, the CCDs may be used to measure x-rays up to 60 keV with good energy resolution ($E/\Delta E \approx 100$ at 60 keV). The difference in detection efficiency between two CCD cameras is small (5.6% at 5.89 keV), but the difference in fraction of the single pixel event between them is much larger (25% at 8.04 keV). The obtained small relative error of detection efficiency (2.4% at 5.89 keV) makes the high accurate measurement of x-ray yield possible in the laser plasma interaction studies. Based on the discrete calibration results, the calculated detection efficiency with XOP can be used for the whole range of 5 keV–30 keV.

Keywords: hard x-ray detector, single photon counting CCD, calibration, laser plasmas

PACS: 52.38.–r, 52.59.Px, 52.70.La, 07.85.Nc **DOI:** 10.1088/1674-1056/26/2/025204

1. Introduction

Studies of hard x-rays are very important in both intense short pulse laser plasma interaction and conventional inertial confinement fusion (ICF) research. In ICF experiment, hot electrons generated in many nonlinear processes, such as stimulated Raman scattering, play a negative role because they preheat the nuclear fuel and lead to less effective compression of the fuel. The hard x-rays induced by the hot electrons have been studied for many years and proved to be very useful in understanding some nonlinear processes in ICF. On the other hand, intense short pulse laser easily produces much more abundant energetic electrons with energy up to GeV. The energetic electrons can produce intense hard x-ray pulse via many processes, such as line emission,[1] bremsstrahlung,[2] betatron radiation,[3] and Thomson scattering. Quantitative spectroscopic characterization of the hard x-ray source is essential for these fundamental and applied researches.

Rather than being used as an imaging component, single photon counting charge coupled device (CCD) has become more and more popular in hard x-ray spectroscopic application in the past twenty years. High sensitivity and good energy resolution of the x-ray CCD camera make possible very low x-ray flux imaging and spectroscopy in many applications,[4–14] such as astronomy,[4] laser plasma physics,[5–10] medical imaging,[11,12] and nuclear physics.[13,14] Commercial CCDs specially designed for hard x-ray spectroscopic applications have been available for some years. PI-LCX:1300 CCD camera from Princeton Instruments is one, a very popular one. Characterization of its response to x-rays is important in order to obtain a high accuracy quantitative result in relevant experimental research. Many calibrations and characterizations were carried out for a variety of other CCDs[15–20] by using different x-ray sources. The very preliminary characterization of PI-LCX:1300 CCD camera[21] was also reported.

In the present study, two identical type PI-LCX:1300 CCD cameras are calibrated with quasi-monochromatic x-rays from radioactive sources and a conventional x-ray tube. Taking a similar event reconstruction method reported[5,18,22,23] in the literature, which we name the "threshold method", a computer code of multi-pixel analysis and event-distinguishing capability is obtained. The energy resolution, the fraction of multi-pixel events as a function of x-ray energy, detection ef-

*Project supported by the Science Foundation of China Academy of Engineering Physics (Grant Nos. 2013A0103003 and 2012B0102008) and the National High-Tech Inertial Confinement Fusion Committee of China.

†Corresponding author. E-mail: jminhong@126.com

© 2017 Chinese Physical Society and IOP Publishing Ltd

ficiency, and consistence of the two CCD cameras are obtained. The measured detection efficiencies are compared with a Monte Carlo calculation (with XOP[24] software) and the data from manual. We find that PI-LCX 1300 CCDs may be used for x-rays up to 60 keV with a good energy resolution $E/\Delta E = 82$, when the multi-pixel event analysis is carried. The calibrated PI-LCX:1300 CCD is used in Copper K-shell line emission experiments with a high power femtosecond laser. The K_α conversion efficiency is obtained with high accuracy. The high precision measurement of x-ray yields is critical in drawing physical conclusion in these laser plasma experiments.

2. Calibration experiments

Monochromatic x-rays are appropriate to calibrate CCD response because photon pileup can be easily distinguished from the known x-ray energy. Two PI-LCX:1300 CCDs (CCD I and CCD II) were calibrated with six radioactive sources and a conventional x-ray tube. Generally, the radioactive sources are quasi-monochromatic x-ray sources because they have multi separate emission lines. The parameters of employed radioactive sources are listed in Table 1. All these radioactive sources are from German Physikalisch Technische Bundesanstalt (PTB). The radioactivity data and their uncertainties listed in Table 1 are from the product datasheet.

Table 1. Radioactive sources employed in the calibration experiment.

Nuclides	Half life	Energy/keV	Probability/%	Radioactivity/10^4 s^{-1}
^{55}Fe	2.7a	5.89, 6.49	24.9, 3.4	7.33±0.22
^{109}Cd	464d	3.1, 21.99, 22.16, 24.9	10.34, 29, 54.7, 15.14	6.05±0.14
^{133}Ba	10.5a	4.53	14.5	8.56±0.09
^{152}Eu	13.6a	5.64	12.7	4.08±0.06
^{241}Am	432.2a	13.76, 13.95, 17.54, 21.01, 59.54	1.08, 11.93, 18.61 4.82, 35.9	5.35±0.06

The energies of x-rays emitted from the nuclides vary from 3.1 keV to 59.54 keV, which covers the nominal working range of the CCD from 2 keV to 30 keV. The ^{241}Am (sealed) has a thick window which is almost transparent to 59.54-keV photons but blocks low energy photons. A magnet was installed between the radioactive source and the CCD camera to turn away possible β rays. Exposure time was set to be 60 s or 90 s due to relatively weak radioactivity. A conventional x-ray tube working at 15 kV/20 mA with a copper target provided a "pure" K_α line emission at 8.04 keV by filtering out the copper K_β line and the bremsstrahlung with a combination of a 200-μm copper foil and a 150-μm nickel foil. By using the x-ray tube, it was possible to directly compare CCD I with CCD II in their response to photons at exact 8.04 keV, which were produced in our laser plasma experiment. In calibration experiment, the photon flux was always regulated to make pileup effect negligible. The CCDs worked at −40 °C to minimize the CCD thermal noise.

3. Characteristics of PC-LCX:1300 CCD

PI-LCX:1300 CCD is a front-illuminated CCD (FI CCD). For FI CCDs, x-rays irradiate the front side of pixel where collecting electrodes are located. The majority of detected x-rays are absorbed at the locations close to the electrodes, leading to relatively small final charge clouds. The array of CCD is 1340×1300. A 50-μm silicon absorption layer provides good detection efficiency for 2-keV to 30-keV x-rays. With 20 μm×20 μm pixels, it also provides high spatial resolution. A thin beryllium window seals the CCD chip for deep cooling and reduces background by filtering out low energy photons. The CCD intrinsic noise is related to the energy resolution of the CCD. Energy resolution of single photon counting CCD camera for the Fano-limit[25] case is expressed as

$$\Delta E = 2.35 \times 3.65 \sqrt{\sigma_{\text{thermal}}^2 + \sigma_{\text{readout}}^2 + F_{\text{f}} \times h\nu/3.65}, \quad (1)$$

where ΔE is the full width at half maximum (FWHM) of the signal, F_{f} is the Fano factor (typical value is 0.117), σ_{thermal} and σ_{readout} are the thermal noise and the readout noise (both units are electron number), and $h\nu$ is the energy of incident x-ray photons in units of eV. We have checked the intrinsic σ_{thermal} and σ_{readout} of the CCDs. Obviously, the σ_{thermal} is strongly dependent on chip temperature and exposure time, but σ_{readout} is only related to the frequency of data readout. The lower the readout frequency, the smaller the readout noise is. The background noise (no impinging x-rays) of PI-LCX:1300 CCD is $\exp\left[-\frac{1}{2}\left(\frac{x-x_0}{\sigma}\right)^2\right]$ fitted very well by a Gaussian function, where x_0 is the mean value and σ is the standard deviation. Typically, the x_0 equals several hundred ADUs (analogy-digital-unit) and the σ equals several ADUs. After a subtraction of this background with another "background image" measured under identical conditions as those used to acquire the first background data, the remaining noise is fitted again by a Gaussian function, which results in a smaller σ (about half initial value) and an x_0 close to zero (about 0.7). The standard deviation of background after this subtraction ($\sigma_{\text{subtraction}}$ in unit of electron numbers) is measured for different exposure times with the experiment parameters of −40 °C, 100-kHz readout rate, low noise. The results are listed in Table 2.

Table 2. Dependences of CCD background (after "DC background" subtraction) on exposure time with 100-kHz readout rate. For gain 1, 1 ADU represents 5.02 electrons, for gain 2, 1 ADU refers to 2.57 electrons.

Exposure time	1 ms	10 ms	50 ms	100 ms	5 s	5 s	60 s
Gain	1	1	1	1	1	2	2
$\sigma_{\text{subtraction}}$/e	10.5	85	10.5	8.5	15.1	19.8	46.0

It is clear that when the exposure time is less than 100 ms, the $\sigma_{\text{subtraction}}$ is almost constant while for longer exposure time (5 s and 60 s), the $\sigma_{\text{subtraction}}$ increases with exposure time. This is not surprising because the thermal noise is small compared with the constant readout noise when exposure time is short enough. The thermal noise can be estimated from a formula $\sigma_{\text{thermal}} \approx 0.5 \times \sqrt{I_{\text{dark}} \times t_{\text{exposure}}}$. The σ_{thermal} is less than 1.6 electrons for the 100 e/pixel/s dark current when the exposure time is less than 100 ms, while the readout noise is 5.4 electrons (root mean square value) (RMS value) according to the manual. For longer exposure time (5 s and 60 s), the σ_{thermal} is larger than the σ_{readout}, therefore the $\sigma_{\text{subtraction}}$ increases with exposure time increasing.

4. Multi-pixel analyzing and event-distinguishing method

All CCDs for x-ray spectroscopic application work in a so-called single photon counting mode. In this mode, incoming x-ray flux is adjusted to make "pileup" negligible (here "pileup" means that more than one photon is absorbed by a pixel). Because the number of electron-hole pairs produced by absorption of an x-ray photon in CCD depletion layer is proportional to the x-ray energy, the energy of incoming x-ray can be obtained by measuring the number of free electrons. In such a way, the energy spectrum of incoming x-ray can be reconstructed without extra dispersive device. Since collected electron clouds are not infinitely small, the electrons belong to a charge cloud may be split into neighbor pixels during collection. This kind of electron splitting leads to so-called multi-pixel event. For multi-pixel events, the number of all electrons for one event is proportional to the incoming x-ray energy. Many studies[25–31] have been performed to understand the detailed processes of production, drift, diffusion, recombination and collection of excited electron clouds. The experiment[32–34] with mesh method verified the relationship between the transverse position of x-ray interaction with the pixel and the type of multi-pixel event. The simulations[35,36] successfully reproduced the measured fraction of each kind of multi-pixel event as a function of x-ray energy.

To construct spectra from raw CCD data, we use a "threshold method". In this method, a threshold is picked up to determine the count of each pixel caused by incoming x-rays or by CCD noise. The distinguishing test is not absolutely correct for each pixel because the counts induced by x-rays may be smaller than that induced by the noise, especially for the multi-pixel event whose pixels may have a small count due to the small splitting of electron clouds. However, the "threshold method" is still practicable because the percentage of error can be controlled under a certain level by choosing an appropriate threshold due to the statistical property of the CCD background. As discussed in Section 3, the background can be approximated well by a Gaussian distribution with rather small standard deviation (σ). For the Gaussian distribution, the probabilities of pixel with the count larger than the threshold are only 1.3×10^{-3}, 3.2×10^{-5}, and 3×10^{-8}, when the thresholds are set to 3σ, 4σ, and 5σ respectively. The slight increase of the threshold can lead to the dramatic decrease of the probability of fake signals (i.e., the misjudgment of a noise as a signal) at the expense of some increase of fake noise (i.e., the misjudgment of a signal as a noise). A fake signal may lead to a bigger event and the up-shift of the x-ray energy, while a fake noise may lead to a smaller event and the down-shift of x-ray energy. A low energy tail in the reconstructed spectrum due to the down-shift of x-ray energy is quite obvious when the threshold is set to be 5σ. Generally, a threshold between 3σ and 5σ is appropriate choice, depending on particular data analysis purpose.

Figure 1 presents a portion of a raw CCD data obtained with ^{241}Am source, showing each kind of multi-pixel event. As shown in Fig. 1, only pixels of direct connection at edges, rather than connection at corners, belong to one event. This classification has been verified and adopted in previous study.[37] The calibration data show that there are four types of multi-pixel events (1–4 pixel event) when x-ray photon energy is less than 22 keV. However, for 59-keV x-ray photons, 5-pixel and 6-pixel events exist in addition to 1–4 pixel events, though the fractions of 5-pixel and 6-pixel events are still small (five percent, see Table 3).



Fig. 1. (color online) A portion of raw CCD data obtained with ^{241}Am source showing each kind of multi-pixel event.

Figure 2 shows the histograms of raw CCD data and the data after the multi-pixel analysis and event-distinguishing with threshold method. The data are obtained with a Cu laser plasma filtered by a 100-μm Cu foil and a sealed ^{241}Am source. For Cu laser plasma, the threshold is set to be 3σ. The number of pixels of the above threshold counts induced

by x-rays is about twenty-one thousands, giving an exposure rate of 0.9%. In Fig. 2(a), the large plateau from 1 keV to 7 keV is obviously not real because of the very low transmittance of a 100-μm Cu foil for x-rays below 7 keV. This plateau is present due to the distribution of the electron clouds among adjacent pixels. The reconstructed spectrum in Fig. 2(b) correctly shows two emission lines only and the plateau disappears completely. The energy resolution at 8.04 keV for 1 pixel event is 170 eV, which is in excellent agreement with 174 eV calculated from formula (1) for an exposure time of 5 s. If all pixel events are used, the energy resolution at 8.04 keV drops to 240 eV. On the other hand, even though the detection efficiency for 59.5-keV x-rays from ^{241}Am is very low, the 59.5-keV line becomes clearly visible in the reconstructed spectrum as shown in Fig. 2(d). In contrast, the 59.5-keV line is not visible at all in the histogram of raw data in Fig. 2(c).

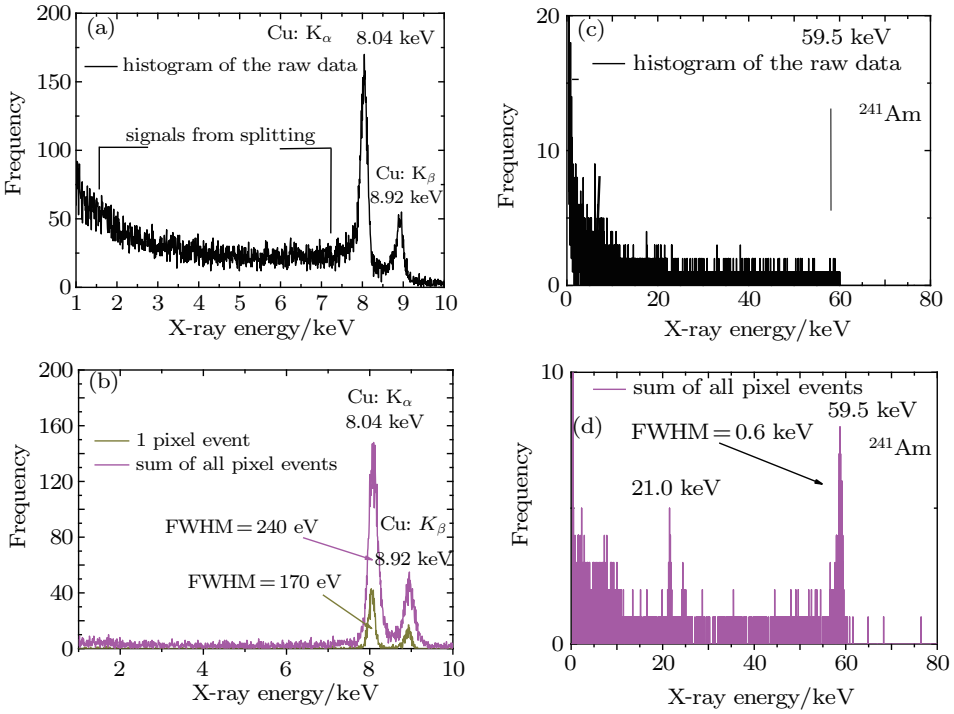


Fig. 2. (color online) Histograms of the CCD counts before ((a) and (c)) and after ((b) and (d)) the multi-pixel analyzing and event-distinguishing treatment for Cu laser plasmas and ^{241}Am sources.

5. Fraction of multi-pixel events as a function of x-ray energy

Using the "threshold method" discussed in Section 4, fractions of all kinds of events are calculated from the raw CCD data. The fractions at five discrete x-ray photon energy points for CCD I and fraction at 8.04 keV for CCD II are listed in Table 3. All data in Table 3 are obtained with 3σ threshold. In addition, pileup probabilities for all cases are less than 0.3%. The data in Table 3 show that each multi-pixel event occurs with different probabilities for x-rays of different energies. Generally, the fraction of small pixel event is larger for smaller energy x-rays. When x-ray photon energy increases from 5.9 keV to 59.5 keV, the fraction of single pixel event monotonously decreases from 55% to 5%, but the fraction of 4-pixel event monotonously increases from 4% to 35%.

Occurrence of multi-pixel event is due to limited size of collected electron cloud. The location where the x-ray is absorbed in the silicon layer in the direction parallel to pixel surface directly determines the type of multi-pixel event.[34] The location near the pixel center results in single pixel event, the location near the pixel edge results in 2-pixel events, and the location near the pixel corner results in 3 and 4 pixel events.

Table 3. Fractions of multi-pixel events for different energy x-rays.

Pixel number of events	CCD I					CCD II
	5.89 keV (^{55}Fe)	8.04 keV (Cu)	13.7 & 13.9 keV (^{241}Am)	22.16 keV (^{109}Cd)	59.54 keV (^{241}Am)	8.04 keV (Cu)
1	55 %	50 %	37%	23%	5%	40 %
2	36 %	39 %	38%	42%	33%	38 %
3	5 %	5 %	12%	12%	23%	9 %
4	4 %	6 %	13%	23%	35%	13 %
5 and 6					5%	

Different collected electron cloud size leads to different fraction of multi-pixel event. Higher energy x-rays produce larger primary electron clouds and are averagely absorbed at deeper position in silicon layer. Using the formula $\Phi_{\text{electroncloud}} = 73 \times \left(E_{\text{photon}}/2.3\ \text{keV}\right)^{1.75}$ nm, the sizes of primary electron clouds are obtained to be 0.4 μm, 1.7 μm, 3.8 μm, and 22 μm for the x-rays of 6 keV, 14 keV, 22 keV, and 60 keV, respectively. Considering longer drift distance to collection electrode for electron clouds produced by higher energy x-rays, the size of final collected electron clouds becomes even bigger for higher energy x-rays. Because 22-μm size of primary electron clouds for 60-keV x-rays is already slightly larger than the 20-μm pixel size, the 5% single pixel event for 60-keV photons is a reasonable number. For 5.9-keV x-rays, according to their experimental data of 4% 4-pixel events, the calculated diameter of electron clouds is 5.6 μm by assuming a spherical electron cloud. This result suggests that the diffusion during the drift of electron clouds to the electrode makes the final collected electron cloud much larger than 0.4-μm electron cloud. Like the previous work,[36,38] complete quantitatively explanation to data in Table 3 needs detailed simulations, which will be carried out in the future.

6. Detection efficiency

Detection efficiency (ε_{d}) is one of most important parameters of single photon counting CCD spectrometer. The detection efficiency is defined as $\varepsilon_{\text{d}} \equiv N_{\text{d}}/N_{\text{i}}$, where N_{d} is the detected x-ray photon number, N_{i} is the number of x-ray photon impinging on the CCD beryllium window of the area equal to the area of CCD chip. For the experiment setup, $N_{\text{i}} = A \cdot P \cdot t \cdot (\Omega/4\pi) \cdot tr_{\text{s}} \cdot tr_{\text{f}} \cdot tr_{\text{air}}$, where A is the activity of radioactive source; P is the characteristic photon emission probability; t is the exposure time; Ω is the solid angle for the CCD chip; $tr_{\text{air}}, tr_{\text{f}}, tr_{\text{s}}$ are the transmittances of photons through the given length of air, the protective foil of radioactive source, and the radioactive source itself, respectively. Each measurement is repeated six times. The N_{d} is calculated by the "threshold method" described in Section 4 for each raw datum. All types of multi-pixel events are included in the counting of detected photons. Detection efficiencies at six discrete energy points for CCD I are plotted in Fig. 3, where the error bars represent the statistic errors of six measurements. The detection efficiency curve from the data sheet of the manual is also included in Fig. 3. Theoretical detection efficiency curve is calculated with the XOP software (ver. 2.4). In the XOP calculation, the percentage of deposited x-ray energy within the 50-μm silicon layer behind a 250-μm beryllium filter is treated as the theoretical ε_{d}. The calculated detection efficiency curve is also plotted in Fig. 3.

Figure 3 clearly shows that the ε_{d} depends strongly on x-ray energy. A maximum of ε_{d} curve is located at 5.2 keV. When x-ray energy increases from 2 keV to 5.2 keV, the ε_{d} jumps from 1.5% up to 75%. When x-ray energy increases from 5.2 keV to 30 keV, the ε_{d} drops relatively slowly from 75% down to 1.5%. Explanation to this dependence is very simple. If x-ray energy is too small, very few x-rays can penetrate the beryllium window and be captured by the silicon layer. Contrariwise, if x-ray energy is too big, most x-rays penetrate beryllium window, but only very few of them deposit their energy in the silicon layer, and most of them will just penetrate the silicon layer.

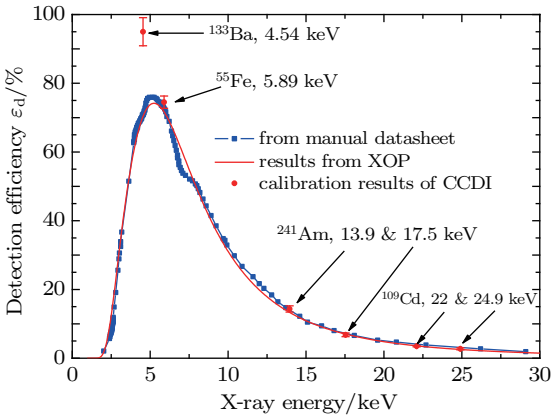


Fig. 3. (color online) Comparison between the calibrated detection efficiencies from the XOP calculation and data from the manual. The anomalously high detection efficiency of the ^{155}Ba at 4.54 keV is due to the strong noise excited by high energy γ rays.

While the other five data from the calibration are in good agreement with the XOP calculations and the data from the manual, there is an exception for the data of ^{133}Ba at 4.54 keV. The calibrated efficiency at this energy point is much higher than the XOP calculation. This disagreement can be explained as follows. While the ^{133}Ba radioactive source emits the characteristic 4.54-keV photons, it also emits a large number of high energy γ rays. The luminescence excited by the high energy γ rays and the scattering of the high energy photons introduce a lot of low energy photons, which mix with the characteristic photons. These inherent noises cannot be accurately calculated and subtracted, which makes the measured ε_{d} significantly larger. A similar problem happens in the cases of ^{152}Eu at 5.64 keV and ^{109}Cd at 3.1 keV, which are not included in Fig. 3.

All calibrated data, together with the XOP calculation results, are collected in Table 4. For ^{55}Fe, which is free from noises induced by high energy γ photons, the measured ε_{d} at 5.89 keV is$(74.5 \pm 1.8)\%$. The 2.4% (1.8/74.5) relative error is almost consistent with the 2.6% relative error calculated from the relative errors of the A, t, and Ω. Considering the experimental error, the calibrated ε_{d} and XOP calculation are in very good agreement for all five energy points between 5 keV to 25 keV. On the other hand, the calibrated ε_{d} at 4.54 keV for ^{133}Ba is 35% larger than the XOP results, which is due to the reason discussed in the previous paragraph. At 59.5 keV, the

calibrated efficiency ($(8.8\pm4.4)\times10^{-4}$) and XOP calculation results (2.4×10^{-3}) are inconsistent, though the reconstructed spectrum in Fig. 2(d) shows clearly distinguished peak. This inconsistency needs further investigating in the future.

The comparison between two CCDs shows an important result which attention should be paid to in usage of the CCDs. The detection efficiencies at 5.89 keV for two CCDs as shown in Table 4 differ by 5.6%. However, the difference in fraction of single pixel event between them is much larger. As shown in Table 3, the difference at 8.04 keV reaches up to 25%. According to the previous discussion, we suggest that the silicon layer of CCD II is thicker than that of CCD I, because thicker silicon layer leads to larger detection efficiency, in the meanwhile, smaller fraction of single pixel event. These results justify the necessity of including all multi-pixel events to reduce the error in comparing their results.

Table 4. Summary of detection efficiencies. The error bars in the third and the sixth columns are the standard deviations of six measurements at each energy points.

Nuclides	X-ray energy/keV	Detection efficiency from calibration for CCD I/%	Detection efficiency from XOP calculation/%	Detection efficiency from data sheet/%	Detection efficiency from calibration for CCD II/%
^{133}Ba	4.53	95.0±4.1	70.4	70.8	
^{55}Fe	5.89	74.5±1.8	71.7	72.8	78.5±2.6
^{241}Am	13.9	14.3±0.9	13.5	14.5	
^{241}Am	17.5	6.81±0.54	7.01	6.8	
^{109}Cd	22.1	3.48±0.19	3.57	3.9	
^{109}Cd	24.9	2.75±0.32	2.53	2.85	

7. Summary

In this work, the detailed calibration of the PI LCX 1300 single photon counting CCD camera is carried out. The multi-pixel analyzing and event-distinguishing method is built and applied successfully to processing the calibration data. The calibrated detection efficiencies of high precision (relative error$<$ 2.5% at 5.89 keV) are obtained. The calibrated $\varepsilon_{\rm d}$ and XOP calculation are in very good agreement for x-ray of energy larger than 5.9 keV within the experimental errors. Due to strong dependences of single pixel event on x-ray energy and on particular CCD camera, it is important to take all sorts of multi pixel events into account in the measurement of the hard x-ray yields. Based on the calibration results, the calculated detection efficiency with XOP at other uncalibrated energy points can be confidently used for x-ray energies between 5.9 keV and 30 keV. However, more calibrations are necessary in the future for x-ray energies between 1.5 keV to 4.65 keV.

Compared with crystal hard x-ray spectrometer, which is also commonly used in laser plasma experiment, the single photon counting CCD spectrometer has advantages in measurement range, detection efficiency, accuracy of detection, and alignment. The drawback of single photon counting CCD spectrometer is its lower energy resolution, and the typical energy resolution of crystal spectrometer can easily reach better than one thousand. A weeping magnetic field in front of CCD is also necessary in order to bend away the hot electrons usually present in the intense short pulse laser plasma experiment.

References

[1] Chen L M, Kando M, Xu M H, Li Y T, Koga J, Chen M, Xu H, Yuan X H, Dong Q L, Sheng Z M, Bulanov S V, Kato Y, Zhang J and Tajima T 2008 *Phys. Rev. Lett.* **100** 045004

[2] Stoeckl C, Theobald W, Sangster T C, Key M H, Patel P, Zhang B B, Clarke R, Karsch S and Norreys P 2004 *Rev. Sci. Instrum.* **75** 3705

[3] Rousse A, Phuoc K T, Shah R, Pukhov A, Lefebvre E, Malka V, Kiselev S, Burgy F, Rousseau J P, Umstadter D and Hulin D 2004 *Phys. Rev. Lett.* **93** 135005

[4] Francis H J, Flint I, Holland A D and Wells A 1992 *Institute of Physics Conference Series* **121** pp. 9–16

[5] Fourment C, Arazam N, Bonte C, Caillaud T, Descamps D, Dorchies F, Harmand M, Hulin S, Petit S and Santos J J 2009 *Rev. Sci. Instrum.* **80** 083505

[6] Arora V, Vora H S, Chakera J A, Tayyab M, Naik P A and Gupta P D 2013 *Journal of Instrumentation* **8** P01010

[7] Stoeckl C, Theobald W, Sangster T C, Key M H, Patel P, Zhang B B, Clarke R, Karsch S and Norreys P 2004 *Rev. Sci. Instrum.* **75** 3705

[8] Fourmaux S, Corde S, Phuoc K T, Leguay P M, Payeur S, Lassonde P, Gnedyuk S, Lebrun G, Fourment C, Malka V, Sebban S, Rousse A and Kieffer J C 2011 *New J. Phys.* **13** 033017

[9] Labate L, Giulietti A, Giulietti D, Koster P, Levato T, Gizzi L A, Zamponi F, Lubcke A, Kampfer T, Uschmann I and Forster E 2007 *Rev. Sci. Instrum.* **78** 103506

[10] Landen O L, Farley D R, Glendinning S G, *et al.* 2001 *Rev. Sci. Instrum.* **72** 627

[11] Labate L, Levato T, Galimberti M, Giulietti A, Giulietti D, Sanna M, Traino C, Lazzeri M and Gizzi L A 2008 *Nucl. Instrum. Method A* **594** 278

[12] Ott R, Macdonald J and Wells K 2000 *Phys. Med. Biol.* **45** 2011

[13] Ishiwatari T, Beer G, Bragadireanu A M, *et al.* 2006 *Nucl. Instrum. Method A* **556** 509

[14] Cargnelli M, Fuhrmann H, Giersch M, Gruber A, Hirtl A, Ishiwatari T, Kienle P, Marton J and Zmeskal J 2004 *Nucl. Instrum. Method A* **535** 389

[15] Lumb D H 1990 *Nucl. Instrum. Method A* **290** 559

[16] Howe J, Chambers D M, Courtois C, Forster E, Gregory C D, Hall I M, Renner O, Uschmann I and Woolsey N C 2006 *Rev. Sci. Instrum.* **77** 036105

[17] Nishiuchi M, Koyama K, Awaki H, Tsuru T, Sakano M, Hamaguchi K, Murakami H, Tsunemi H, Hayashida K, Kitamoto S, Miyata E, Dotani T, Ozaki M, Bautz M, Doty J, Kissel S, Foster R and Ricker G 1999 *Nucl. Instrum Method A* **436** 79

[18] Labate L, Galimberti M, Giulietti A, Giulietti D, Gizzi L A, Tomassini P and Di Cocco G 2002 *Nucl. Instrum Method A* **495** 148

[19] Kraft R P, Nousek J A, Lumb D H, Burrows D N, Skinner M A and Garmire G P 1995 *Nucl. Instrum. Method A* **366** 192

[20] Bootsma T M V, Van Zwet E J, Brinkman A C, Den Herder J W, De Jong L, De Korte P and Olsthoorn S M 2000 *Nucl. Instrum. Method A* **439** 575

[21] Maddox B R, Park H S, Remington B A and Mckernan M 2008 *Rev. Sci. Instrum.* **79** 10E924

[22] Chun H J, Bowles J A, Branduardi-Raymont G and Gowen R A 1996 *Nucl. Instrum. Method. A* **376** 254

[23] Levato T, Labate L, Galimberti M, Giulietti A, Giulietti D and Gizzi L A 2008 *Nucl. Instrum. Method A* **592** 346

[24] http://www.esrf.eu/Instrumentation/software/data-analysis/xop2.4

[25] Lumb D H, Chowanietz E G and Wells A 1987 *Opt. Eng. (Bellingham)* **26** 773

[26] Hopkinson G R 1987 *Opt. Eng.* **26** 268766

[27] Tsunemi H, Hiraga J and Miyata E 2002 *Nucl. Instrum. Method A* **477** 155

[28] Pavlov G G and Nousek J A 1999 *Nucl. Instrum. Method A* **428** 348

[29] Tsunemi H, Hiraga J, Mori K, Yoshita K and Miyata E 1999 *Nucl. Instrum. Method A* **436** 32

[30] Prigozhin G, Rasmussen A, Bautz M and Ricker G 1998 *X-Ray Optics, Instruments, and Missions, Proc. SPIE* **3444**, July 19, 1998, San Diego, CA, USA, p. 267

[31] Fowler R F, Ashby J V and Greenough C 2000 *Nucl. Instrum. Method A* **450** 75

[32] Hiraga J, Tsunemi H, Yoshita K, Katayama H and Hayashida K 1999 *Euv, X-Ray, and Gamma-Ray Instrumentation for Astronomy X*, p. 291

[33] Hiraga J, Tsunemi H, Yoshita K and Miyata E 1999 *Astron. Nachr.* **320** 371

[34] Hiraga J, Tsunemi H and Miyata E 2001 *Jpn. J. Appl. Phys. Part 1-Regular Papers Short Notes & Review Papers* **40** 1493

[35] Mccarthy K J, Owens A, Holland A D and Wells A A 1995 *Nucl. Instrum. Method A* **362** 538

[36] Townsley L K, Broos P S, Chartas G, Moskalenko E, Nousek J A and Pavlov G G 2002 *Nucl. Instrum. Method A* **486** 716

[37] Tsuneml H, Hiraga J, Yoshita K and Kitamoto S 1998 *Jpn. J. Appl. Phys.* **37** 2734

[38] Mccarthy K J, Owens A, Holland A D and Wells A A 1995 *Nuclear Instruments & Methods in Physics Research Section a-Accelerators Spectrometers Detectors and Associated Equipment* **362** 538